Electrochimica Acta 88 (2013) 240–250

Contents lists available at SciVerse ScienceDirect

Electrochimica Acta

journal homepage: www.elsevier.com/locate/electacta

Incorporation of iridium into electrodeposited rhenium–nickel alloys

Maayan Cohen Sagiv[a], Noam Eliaz[a,*,1], Eliezer Gileadi[b,2]

[a] Biomaterials & Corrosion Laboratory, School of Mechanical Engineering & The Materials and Nanotechnologies Program, Tel-Aviv University, Ramat-Aviv 69978, Israel
[b] School of Chemistry, Raymond and Beverly Sackler Faculty of Exact Sciences, Tel-Aviv University, Ramat-Aviv 69978, Israel

ARTICLE INFO

Article history:
Received 31 August 2012
Received in revised form 21 October 2012
Accepted 22 October 2012
Available online xxx

Keywords:
Rhenium–iridium–nickel alloys
Electrodeposition
Induced codeposition

ABSTRACT

Rhenium (Re), a refractory metal that has gained significant recognition as a high performance engineering material, is mostly used in military, aircraft and aerospace applications, as well as for catalysis in the petrochemical industry. However, its performance at high temperature in humid air is limited by the formation of rhenium heptoxide (Re_2O_7), which penetrates the grain boundaries and causes brittleness. Improvement of this is being sought through the incorporation of iridium (Ir) into Re deposits. To this end, suitable plating baths for Re–Ir–Ni coatings were developed. These alloys were deposited from different aqueous solutions on copper substrates under galvanostatic conditions, in a three-electrode cell. The plating bath consisted of iridium tri-chloride, ammonium perrhenate and nickel sulfamate as the electroactive species, and citric acid as the complexing agent. The effects of bath composition and operating conditions on the Faradaic efficiency (FE), partial current densities, as well as on the thickness of the coatings and their composition were studied. Re–Ir–Ni coatings as thick as 18 μm, with Re-content as high as 73 at.% and Ir-content as high as 29 at.%, were obtained, using different plating baths. A mechanism of the electrochemical process was suggested. It was found that both an HCP $Ir_{0.4}Re_{0.6}$ phase and an HCP Ni phase with nanometric crystallites were formed, possibly together with a hexagonal nickel hydride (Ni_2H) phase.

1. Introduction

Rhenium (melting point 3186 °C) is a strong, ductile, refractory metal with a hexagonal close-packed (HCP) crystal structure. Due to its superior mechanical and physical properties [1,2], it has gained significant importance in recent years as a high-performance engineering material, and is widely used in a variety of applications such as aircraft, aerospace, nuclear, electronic, biomedical and catalysis [2].

Despite its unique combination of properties, the performance of Re in high-temperature oxidizing environments is limited by the formation of rhenium heptoxide (Re_2O_7), which penetrates the grain boundaries and causes brittleness. Thus, one of the major current challenges is to develop Re-based coatings that can perform in high-temperature oxidizing environments. This could be of crucial importance for aircraft and aerospace applications, where extended thermal and oxidation limits of materials are the key factor to high performance and longevity of the products.

Iridium (melting point 2447 °C) is currently used as an oxidation-resistant coating for Re at high temperatures. Iridium-coated Re nozzles are used in aerospace applications for small chemical rockets and resistojet thrusters [3]. A combustion chamber composed of Re substrate and Ir coating has already been demonstrated as a successful alternative, which is stable for extended lifetimes at higher temperatures (up to 2200 °C) [4,5]. NASA has reported the development of Ir-coated Re rocket chamber technology, allowing an increase in satellite life from 12 to 15 years, and gaining 30–60 M$ in the added revenue per satellite [6]. Among other coating processes, Reed et al. claimed that chemical vapor deposition (CVD) is the only established process for the fabrication of Ir-coated Re combustion chambers [4]. However, some aspects such as high costs, low deposition rates, high deposition temperature and impurity incorporation into the films still remain of major concern [7].

A new approach is being sought through the incorporation of Ir, which has high oxidation resistance and thermal stability at high temperatures, into electrodeposited Re alloys. The objectives of the current study were to develop suitable plating baths for electroplating of Re–Ir-based coatings and to suggest a mechanism for the deposition process. Next we determined the effect of plating bath chemistry and operating conditions on the uniformity, thickness, chemical and phase composition of these coatings.

* Corresponding author. Tel.: +972 3 640 7384; fax: +972 3 640 6648.
E-mail address: neliaz@eng.tau.ac.il (N. Eliaz).
[1] ISE member.
[2] ISE fellow.

0013-4686/$ – see front matter © 2012 Elsevier Ltd. All rights reserved.
http://dx.doi.org/10.1016/j.electacta.2012.10.094

2. Experimental

2.1. Plating bath chemistry

Iridium–rhenium–nickel alloys were electroplated from aqueous solutions containing 17–45 mM $IrCl_3$ (Iridium(III) chloride hydrate, Alpha Aesar #11030), 17–136 mM NH_4ReO_4 (ammonium perrhenate, Sigma–Aldrich #316954), and 17–136 mM $Ni(NH_2SO_3)_2$ (nickel(II) sulfamate, Sigma–Aldrich #262277) as the electroactive species, and 17–136 mM $C_6H_8O_7$ (citric acid, Alpha Aesar #A10395) as the complexing agent. All components were dissolved in deionized water (Direct-Q3, Millipore, theoretical resistivity 18.2 MΩ cm).

The experiments were conducted at pH = 5.00 ± 0.05. The pH was measured before and after the experiment by means of pH meter 510 from Eutech Instruments, and was adjusted at room temperature to the desired value by additions of NaOH and, when necessary, small amounts of H_2SO_4. The specific conductivity of the solution was 7–20 mS cm^{-1}. The volume of electrolyte in the cell was about 10 cm^3. Each experiment was conducted in a fresh solution.

Iridium(III) chloride, the most commonly available compound of Ir, is soluble in water, albeit very slowly. Ammonium perrhenate is the commercially most available salt of Re. Its solubility in water is 215 mM at 20 °C, compared to the lower solubility of potassium perrhenate ($KReO_4$, 37 mM at 21.5 °C) [1]. Nickel(II) sulfamate is a salt of the strong monobasic sulfamic acid (NH_2SO_3H). Its incorporation in Ni and other plating baths usually yields higher throwing power, as well as reduced porosity and reduced residual stresses in the deposit [8]. Citric acid is a commonly used complexing agent. It has three carboxylic groups and one alcoholic group. It is deprotonated gradually from a neutral molecule to a series of negatively charged ions (from −1 to −4) as the pH is increased. Citrate was reported to form stable complexes with Ni and Re, which affects the deposition of their alloys [9,10].

2.2. Operating conditions

In this work, a small, single-compartment, three-electrode cell was used. A sheet of copper with an exposed surface area of $A = 1.57\ cm^2$ was used as the working electrode (WE). Two platinum sheets were used as the anode (counter electrode, CE), and were placed about 0.5 cm away from both sides of the cathode. The diameter of the counter electrode was 1 cm. The ratio between the volume of the solution and the area of the working electrode was 10/1.57 = 6.37 cm. For all experiments, a saturated Ag/AgCl/KCl reference electrode (RE) was used.

A Princeton Applied Research model 263A Potentiostat/Galvanostat was used to control the applied current density at 50 mA cm^{-2}. In earlier work in our laboratory it was observed that increasing the current density above this value tends to produce spongy deposits and lowers the Re-content in the deposit [11].

The cathode was weighed before and after each experiment, with a resolution of ±0.1 mg. The average FE was calculated from the mass gained, the charge passed and the chemical composition of the deposit, as determined by energy dispersive spectroscopy (EDS):

$$\mathrm{FE} = \frac{w}{It} \sum \frac{c_i n_i F}{M_i} \tag{1}$$

where w is the measured weight of the deposit (g), t is the deposition time (s), I is the total current passed (A), c_i is the weight fraction of the element (Re, Ir or Ni) in the ternary alloy, n_i is the number of electrons transferred per atom of each metal (n_i = 7, 3, and 2 for Re, Ir and Ni, respectively), M_i is the atomic mass of the relevant elements (186.2, 192.2 and 58.71 g mol^{-1} for Re, Ir and Ni, respectively), and F is the Faraday constant.

The partial deposition current densities were calculated from the mass gained and the chemical composition of the deposit, using the equation:

$$j_i = \frac{w}{At} \frac{c_i n_i F}{M_i} \tag{2}$$

where j_i is the partial current density of element i (mA cm^{-2}) and A is the surface area of the cathode (cm^2).

In certain favorable cases the thickness of the coatings was measured on metallographic cross-section images, in others it was calculated using the equation:

$$h = \frac{w}{A} \frac{\bar{V}_a}{\bar{M}} \tag{3}$$

where h is the thickness of the deposit (cm), $\bar{V}_a$ is the average molar volume of each metal (V_a = 8.85, 8.54 and 6.60 $cm^3\ mol^{-1}$ for Re, Ir and Ni, respectively), and $\bar{M}$ is the average atomic mass. The average molar volume and the average atomic mass are calculated according to the atomic fraction of each element in the alloy, as determined by EDS measurements.

Prior to electrodeposition, the working electrode was cleaned with detergent in an ultrasonic bath for 3 min and then immersed in 1:1 nitric acid solution at room temperature for about 1 min to remove the native oxide film on the substrate material. This was followed by repeating the cleaning in the ultrasonic bath for the same period of time.

Before turning on the current, the bath was purged with pure nitrogen for about 15 min. During deposition nitrogen was passed above the solution. In all experiments, the plating bath was operated at a temperature of 70 °C. A MRC B300 thermostatic bath was used to control the temperature to within ±0.05 °C.

Stirring by a magnetic stirrer was applied during plating, in order to maintain the homogeneity of solution and reduce pitting due to accumulation of hydrogen at the surface of the cathode [8]. All experiments were carried out under the same stirring condition in order to maintain similar mass transport conditions near the cathode. However, the solution near the cathode was also inherently stirred by hydrogen bubbles, to an extent that decreases with increasing FE. Electroplating was conducted for 1 h, except when the effects of plating time and the rate of deposition of the Re–Ir–Ni alloys were measured.

2.3. Characterization techniques

The surface morphology of the as-deposited coatings was observed by means of a Quanta 200 FEG ESEM operated in the high vacuum mode. The thickness of selected coatings was measured on metallographic cross-sections using a Docu image analysis software package. The attached liquid-nitrogen-cooled Oxford Si EDS detector was used to determine the atomic composition of the deposits. Each sample was analyzed at five locations, to test uniformity.

X-ray photoelectron spectroscopy (XPS) measurements were performed in ultra-high vacuum (2.5×10^{-10} Torr base pressure) using a 5600 Multi-Technique System (PHI, USA). The samples were irradiated with a monochromatic Al Kα source (1486.6 eV), and the outcome electrons were analyzed using a Spherical Capacitor Analyzer with a slit aperture of 0.8 mm. The samples were analyzed either at the surface or after sputter cleaning with a 4 kV Ar^+ ion gun (sputtering rate on SiO_2/Si was 3.9 nm min^{-1}). The binding energy of adventitious carbon (C 1s) at 285 eV was taken as an energy reference for the measured peaks. In order to identify the elements present at the sample surface, a low-resolution survey spectrum was first taken over a wide energy range (0–1400 eV).

High-resolution spectra were acquired at pass energy of 11.75 eV at increments of 0.05 eV step^{-1}, to allow precise determination of the position of the peak and its shape. Curve-fitting was done with Gaussian–Lorentzian function, by using the 5600 Multi-Technique System software. Two fitting parameters – the position of the peak and its full width at half-maximum (FWHM) – were fixed within less than about ±0.2 eV.

X-ray diffraction (XRD) was used for phase identification. XRD measurements were conducted using a Θ–Θ powder diffractometer from Scintag, equipped with a liquid-nitrogen-cooled germanium solid-state detector and a Cu K_α radiation source ($\lambda = 1.5406$ Å). The structure was determined using the whole-pattern fitting (WPF) and Rietveld refinement methods. Thus, all reflections for each phase were considered, and overlapping reflections could be indexed.

3. Results and discussion

In the framework of this study, over 230 samples were coated under different bath chemistries and operating conditions, and were subsequently characterized. In Section 3.1, the effect of different bath chemistries on the FE, partial current densities and Me-content (where Me stands for Re, Ir and Ni) in the deposited alloy are discussed. Next, Section 3.2 presents the effect of deposition time on the FE, partial deposition current densities and Me-content. Subsequently, in Section 3.3 a possible mechanism for the electroplating of Re–Ir–Ni alloy is suggested. Finally, the characterization of selected coatings by means of ESEM, XPS and XRD is analyzed in Section 3.4.

3.1. The effect of bath chemistry

3.1.1. Characterization of the solution

During deposition, a gradual change in the color of the solution, from yellow-greenish brown, through green, to deep dark blue-green, was observed. There was no further change in color after turning off the current. This change in color was observed only in solutions containing Ir ions, and can be attributed to the oxidation of Ir^{3+} to Ir^{4+} at the anode. To confirm this assumption, a simple experiment was conducted in agar–agar gel at room temperature. The yellowish green solution was added, and a current density of 50 mA cm^{-2} was applied between two Pt wires, which were used as working and counter electrodes, respectively. A dark blue spot was observed around the anode. At the cathode there was no change in color. This observation distinctly showed that the blue color is associated with the formation of Ir^{4+} complexes. Colorful solutions of iridium chloride have been reported in the literature [12–16].

3.1.2. The effect of the concentration of citrate ions in the bath

The effect of the stoichiometric concentration of citric acid on the partial current densities, the FE and the composition of the alloy is shown in Fig. 1. The concentrations of iridium, rhenium and nickel ions in the bath were 34, 23, and 34 mM, respectively. The role of citrate as a complexing agent in both W–Ni and Re–Ni systems was described in detail in previous works [1,8,11]. It was found that citric acid could form complexes not only with the positive Ni^{2+} ions, but also with the negative WO_4^{2-} and ReO_4^- ions. An increase in the concentration of citrate has also been reported to result in a decrease in the FE and an increase in W- or Re-content. However, no report on citrate complexes with Ir was found in the literature.

In general, as shown in Fig. 1a, the partial deposition current densities of the three metals were found to go through a shallow maximum, where the concentration of citric acid equals that

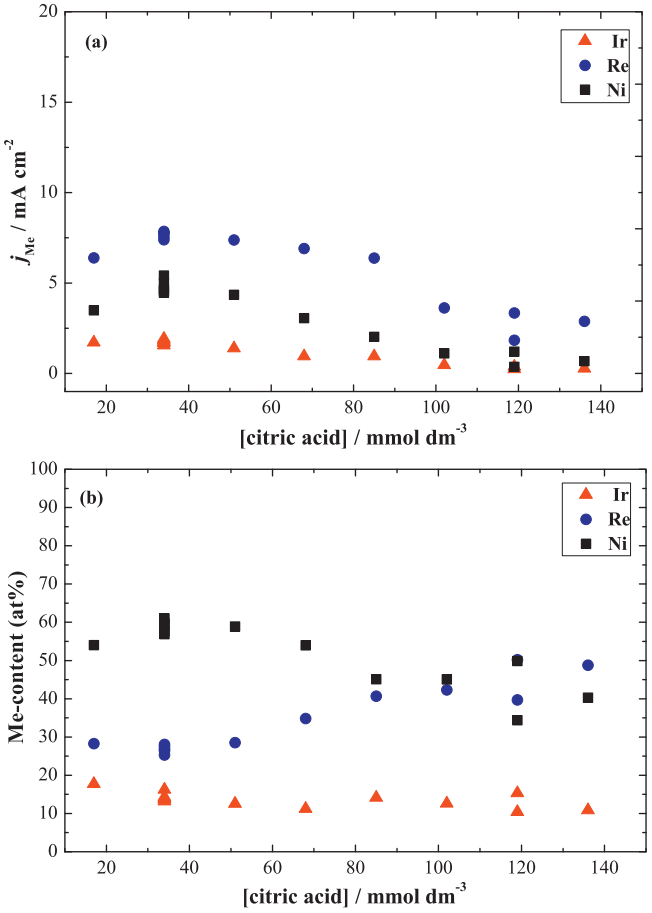

Fig. 1. The partial deposition current densities of Me (a) and the Me-content in the deposit (b), as a function of citrate concentration in solution. The concentrations of $IrCl_3$ (34 mM), NH_4ReO_4 (23 mM), and $Ni(NH_2SO_3)_2$ (34 mM) were kept constant. Plating was conducted for 1 h. The temperature (70.0 ± 0.05 °C), current density (50 mA cm^{-2}) and pH (5.00± 0.05) were the same in all measurements.

of Ni^{2+} and of Ir^{3+} (34 mM each), followed by a gradual decrease with further increase in the concentration of H_3Cit. At the point where the concentration of H_3Cit exceeds slightly the sum of concentrations of the three metal ions (i.e. 91 mM), the partial current density for each of the metals decreased substantially. The FE (not shown here) exhibits a similar trend, decreasing from about 30% to 10%. Finally, Fig. 1b shows the at.% concentration of the three metals in the alloy, as a function of the concentration of H_3Cit. At equal concentrations of Ni^{2+}, Ir^{3+} and H_3Cit, a local maximum in the concentration of Ni in the alloy is observed along with a minimum in the concentration of Re. This behavior is consistent with the dependence of the FE on the concentration of H_3Cit. This observation can be attributed to the fact that Re is a better catalyst for hydrogen evolution than Ni^{2+}. One should bear in mind that, under galvanostatic conditions, an increase in partial current density of one element must be at the expense of another. This may lead to the steady decline in the amount of Ir found in the deposited alloy. At a citrate-to-Ni^{2+} ratio of 1, the concentrations of Ni^{2+} and $[Ni(HCit)_2]^{2-}$ are equal. It is known that the rate of Ni deposition decreases in the order of $Ni^{2+} > Ni(HCit) > [Ni(HCit)_2]^{2-}$. A further increase in the concentration of citrate increases the relative abundance of $[Ni(HCit)_2]^{2-}$, and consequently hinders the rate of Ni deposition. A similar behavior was identified for the Re–Ni system [11].

It should be borne in mind that when a metal ion exists in solution in the form of a complex, its standard potential is shifted cathodically, leading to enhanced hydrogen evolution and a

corresponding decrease in the FE. As the concentration of H_3Cit was increased, the Re-content in the deposited alloy was increased up to 48 at.%. The presence of citrate was reported to markedly enhance the reduction of perrhenate through reversible formation of the complex $(ReO_4H_2Cit)^{2-}$. Vajo et al. [17] claimed that the reduction of ReO^{4-}, which is tetrahedral, to rhenate ReO_3^-, which almost certainly has a coordination number of 6 or higher, involves major changes in the geometry of the coordination sphere of the perrhenate ion. The formation of $(ReO_4H_2Cit)^{3-}$ expands the Re coordination sphere through formation of chelated structures. Consequently, the change in the geometry of the coordination sphere during electroreduction is smaller, and the redox process becomes more reversible. Although at pH 5, used in our experiments, the predominant species is $(ReO_4HCit)^{2-}$, two other complexes of perrhenate, with H_2Cit^- and Cit^{3-}, exist at significant concentrations. Thus, we assume that the same interpretation applies here.

The increase in Re-content may also be related to the formation of a NiCit complex, which inhibits the parallel path for the deposition of Ni. These findings are consistent with the results obtained by Naor et al. [11].

Viewing the Me-content plot in Fig. 1b, one might conclude that the citric acid concentration in the bath has no effect on the deposition of Ir, but this is not the case. Looking carefully at the partial current density for deposition of Ir, a gradual decrease in the rate of deposition is observed. As the H_3Cit-to-Ir^{3+} ratio is increased from 0.5 to 4, the partial current density of Ir is decreased by a factor of 5, indicating that a complex between Ir and citrate is formed.

3.1.3. The effect of the concentration of perrhenate ions in the bath

Fig. 2 shows the effect of ReO_4^- concentration on the Me-content in the deposit and the partial current densities of Re, Ir and Ni. The graphs are plotted as a function of the sum of the concentrations of Ir^{3+} and Ni^{2+} divided by that of ReO_4^-. The analytical concentrations of Ir^{3+}, Ni^{2+} and citric acid were 34 mM each. The partial current density for deposition of Ir seems to be essentially independent of the ratio of $(Ir^{3+} + Ni^{2+})/ReO_4^-$ in solution. However, increasing the ReO_4^- concentration in the bath seems to inhibit the rate of Ni deposition to some extent. A significant decrease in the partial current density for deposition of Re is observed up to $(Ir^{3+} + Ni^{2+})/ ReO_4^- \leq 2.5$, where a saturation value is approached. When viewing the partial current densities for Re, Ir and Ni, one should pay attention to the difference in the number of electrons required for the deposition of each metal. Rhenium requires 7 electrons, Ir – 3, and Ni only 2 electrons. Thus, equal atomic concentrations correspond to partial deposition current density ratio of $i_{Ir} : i_{Re} : i_{Ni} = 1.5 : 3.5 : 1$. With the decrease in perrhenate concentration, the Re-content decreases monotonically by a factor of about 3, whereas the Ni-content is increased by a factor of 2, and the Ir-content is nearly constant. The Re-content in the deposit exceeded that of Ni when the concentration of ReO_4^- was increased beyond the sum of the concentrations of the cations.

In Fig. 2a the partial current density for hydrogen evolution is also shown. When $(Ir^{3+} + Ni^{2+})/ReO_4^- \geq 2.5$, the rate of hydrogen evolution reaches a constant value, corresponding to a FE of 28%, down from its initial value of 48%. This result, combined with the fact that at low concentrations of perrhenate, the rate of Re deposition was not influenced by its concentration, implies that the ReO_4^- ion is not subjected to mass transport limitation. In addition, based on the above observations, it is apparent that the bottleneck for the deposition of the alloy is one of the two cations, whereas the perrhenate anion does not take part in the rate-determining step.

3.1.4. The effect of the concentration of nickel ions in the bath

The effect of the concentration of Ni^{2+} in a bath containing 34 mM Ir^{3+}, 23 mM ReO_4^-, and 34 mM citric acid was examined

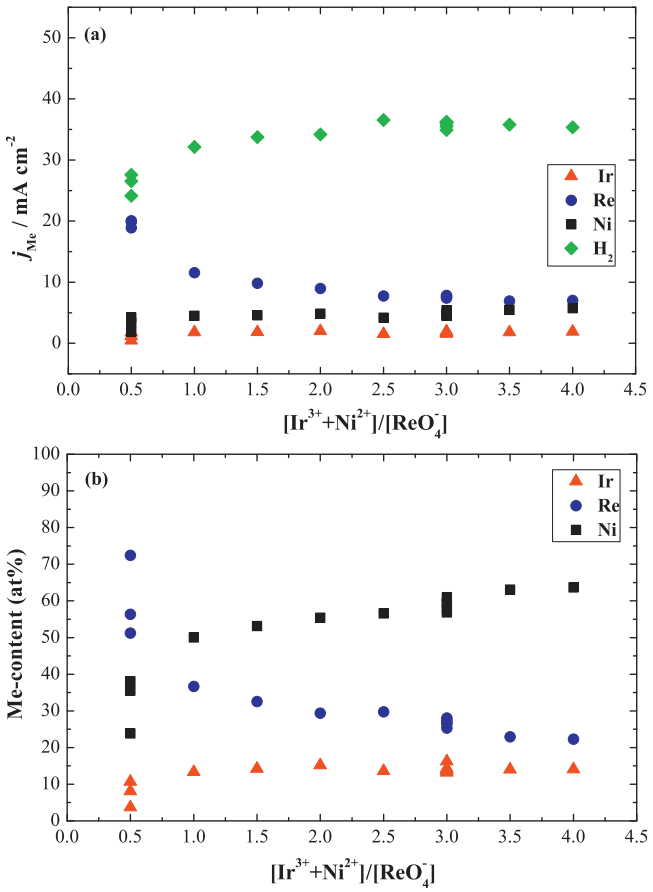

Fig. 2. The effect of the ratio $(Ir^{3+} + Ni^{2+})/ReO_4^-$ on the partial current density of Me (a) and on the Me-content in the deposit (b). The concentrations of Ir^{3+}, Ni^{2+} and citric acid were 34 mM each. Plating was performed under the same conditions as in Fig. 1.

and is shown in Fig. 3. The dependence of the partial current densities and the metal content in the alloy on the concentration of Ni^{2+} is presented in Fig. 3a and b, respectively. Increasing the concentration of Ni^{2+} in the bath resulted in a significant increase of the partial current density for deposition of Re, by a factor of about 5. For a Ni^{2+}/ReO_4^- ratio of unity, an alloy containing 59 at.% Ni, but only 27 at.% Re, is obtained. When this ratio is increased to 3, the Ni-content is decreased to 31 at.% whereas the Re-content approaches a value of 65 at.%. It is evident that the rate of Re deposition is enhanced by the presence of Ni^{2+} in solution but, as seen in Section 3.1.3, not vice versa. Similar catalytic effects were identified for the Re–Ni system in electroless [18] and electroplating [9,11] experiments. Looking at Fig. 3b from right to left, one can see that up to $Cit/Ni \leq 0.5$, the Re-content in the deposit exceeds that of Ni, but above this ratio the reverse trend is observed. At $Cit/Ni \leq 0.5$, the Ni^{2+} ion is free in solution, and most of the citrate is bound to the perrhenate ion. This allows the reduction of Ni^{2+} to its metallic form, which in turn enhances the reduction of ReO_4^- and results in higher Re-content in the alloy.

Regarding the partial current density of Ir, an opposite trend is seen. As the Ni concentration in solution is increased, the partial deposition current density of Ir is steadily decreased to almost zero (0.1 mA cm^{-2}). When the Ni^{2+}/Ir^{3+} ratio is increased from 1 to 3, the partial deposition current density of Ir decreases by a factor of 13, and the Ir-content in the alloy decreases from 14 at.% to only 1 at.%.

In order to extend and further understand the relationship between Ir and Ni species in solution, the following set of experiments was carried out. First, the effect of the Ni^{2+}-to-Ir^{3+} ratio was

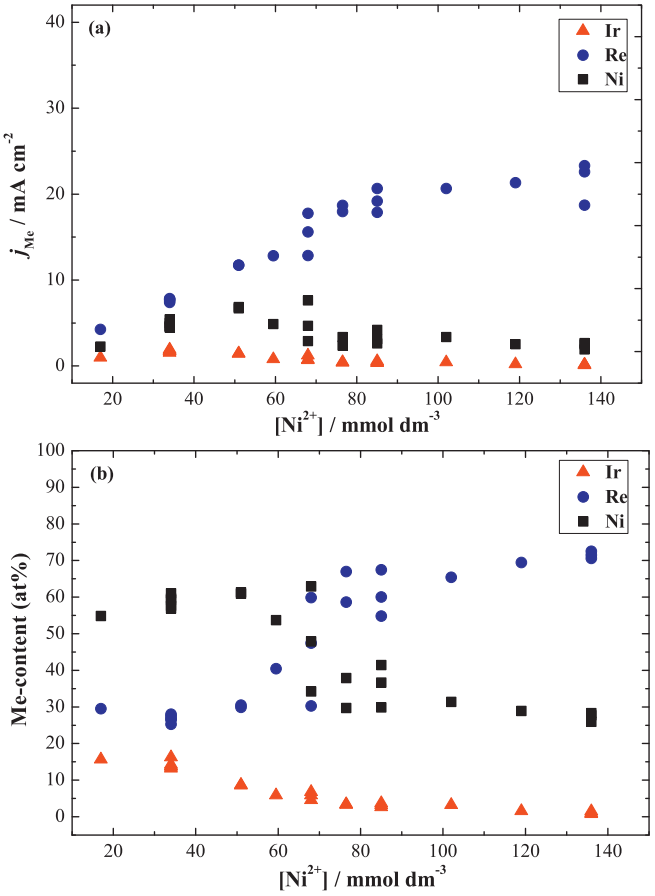

Fig. 3. The dependence of the partial current density of Me (a) and the Me-content in the alloy (b) on the concentration of Ni^{2+} in solution. The Ir^{3+}, ReO_4^- and citric acid analytical concentrations were 34 mM, 23 mM, and 34 mM, respectively. Plating was conducted under the same conditions as in Fig. 1.

studied while the sum of the concentrations of the two cations was maintained constant, at a value of 68 mM. The concentrations of perrhenate and citrate ions in the bath were 23 and 34 mM, respectively.

It is clear from Fig. 4a that as the Ni^{2+}-to-Ir^{3+} concentration ratio in the bath is increased from 0.5 to 3, the Ir-to-Ni ratio in the alloy decreases from 0.35 to 0.1. This observation is consistent with the results shown in Fig. 3b. Thus, it can be concluded that the deposition of Ir and Ni are competing reactions that take place in parallel.

In order to further investigate the relationship between the Ir and Ni ions, the ReO_4^- ion was excluded from the solution. A plating bath containing equal concentrations (34 mM) of Ir^{3+} and Ni^{2+} with varied concentrations of citric acid (17–102 mM) was examined. In Fig. 4b it is seen that, in the absence of perrhenate, the FE is very low, although the partial current densities for Ni and Ir follow the same trend as in the presence of perrhenate.

In Fig. 4c, one should note the very high Ni-content in the alloy (up to 87 at.%) compared to that of Ir, indicating that the deposition of Ni^{2+} is favored. The ratio of Ni-to-Ir content in the deposit increased with increasing concentration of citric acid, going through a maximum at citrate-to-(Ir^{3+} + Ni^{2+}) = 1.

The additional data obtained by the last two experiments, together with the results shown above, support the assumption that perrhenate has no effect on the relationship between Ir and Ni. Thus, the rate-determining step in Re–Ir–Ni deposition seems to be the electrodeposition of Ni, as in the absence of Ir^{3+}. This will be discussed in Section 3.3 below.

3.2. The effect of deposition time

The effect of plating time was studied in the range of 10–80 min, under otherwise identical conditions. The plating bath used in this series of experiments consisted of 34 mM Ir^{3+}, 23 mM ReO_4^-, 34 mM Ni^{2+} and 34 mM Cit.

In Fig. 5a it is shown that with increasing time, the partial current density of both Re and Ni decrease, while that for Ir is very small, but remains essentially constant (Fig. 5b). The FE (calculated from the partial current density for hydrogen evolution) shown in this figure decreased from 46% after 10 min to 23% after 80 min.

In Fig. 5c, the data for the increase of thickness with time of the Re–Ir–Ni alloy follow a linear relationship, up to about 40 min, but tends to level off at longer deposition times. A deposition rate of 14 $\mu m\,h^{-1}$ is obtained. For comparison, a value of 9.5 $\mu m\,h^{-1}$ was reported for the Re–Ni system [10]. The change in slope beyond 40 min is probably associated with partial depletion of the solution, as will be shown below.

The results in Fig. 5a–c indicate that depletion of the metal ions in the bath is taking place. An attempt to evaluate the degree of depletion yielded Fig. 5c, which shows the fraction of each metal ion in solution during plating, relative to its initial concentration. For example, after 80 min of plating, 44% ReO_4^-, 64% Ni^{2+} and only 12% Ir^{3+} were utilized for the alloy deposition. It is evident that the effect of depletion is more pronounced for Ni^{2+} ions in solution, which exhibit a steeper decrease with time. In contrast, a mild decrease with time is identified for the Ir^{3+} ions. It is concluded that depletion of the metal ions during plating can play some role in our system. This effect can be avoided, or at least minimized, either by increasing the volume of the solution or increasing the concentrations of the species in solution. However, it has little or no effect on the discussion of the mechanism of electroplating of the alloy.

3.3. The proposed mechanism of rhenium–iridium–nickel electrodeposition

Understanding the fundamental mechanism of electroplating of Re–Ir–Ni alloys is of great scientific and commercial importance. It is rather complicated because at least four reactions occur simultaneously in parallel. Consequently, the current–potential relationship represents a combination of the contribution of at least four processes, each having its own overpotential, rate constant and partial current density.

A mechanism for the Re–Ni system was proposed by Naor et al. [11]. It was suggested that addition of nickel sulfamate to the solution enhances the rate of deposition of Re through a unique type of electroless plating, in which Ni^{2+} is reduced to its metallic form that is probably adsorbed on the surface. In the next step, the perrhenate ion is reduced chemically to rhenate by the adsorbed Ni atom via the following reactions:

$$Ni^{2+} + 2e^- \rightarrow Ni^0 \quad (4)$$

$$Ni^0 + ReO_4^- + 2H_3O^+ \rightarrow Ni^{2+} + ReO_3^- + 3H_2O \quad (5)$$

and the rhenate ion, ReO_3^-, which is less stable than the perrhenate ion, ReO_4^-, could be reduced electrochemically to metallic Re. The reduction of Ni^{2+} was found to be the rate-determining step. It should be noted that, although most of the current passed may initially be consumed to reduce the divalent ion Ni^{2+}, a significant fraction of these ions are regenerated via reaction (5), instead of being incorporated in the deposited alloy, leading to a low apparent current density for the reduction of Ni^{2+}. Reduction at open-circuit of perrhenate by Sn to metallic Re and Re oxides has also been observed [19]. Based on the experimental data acquired in this work and the detailed analysis of the results, it is reasonable to assume, as a starting point for the study of electroplating of Re–Ir–Ni alloys,

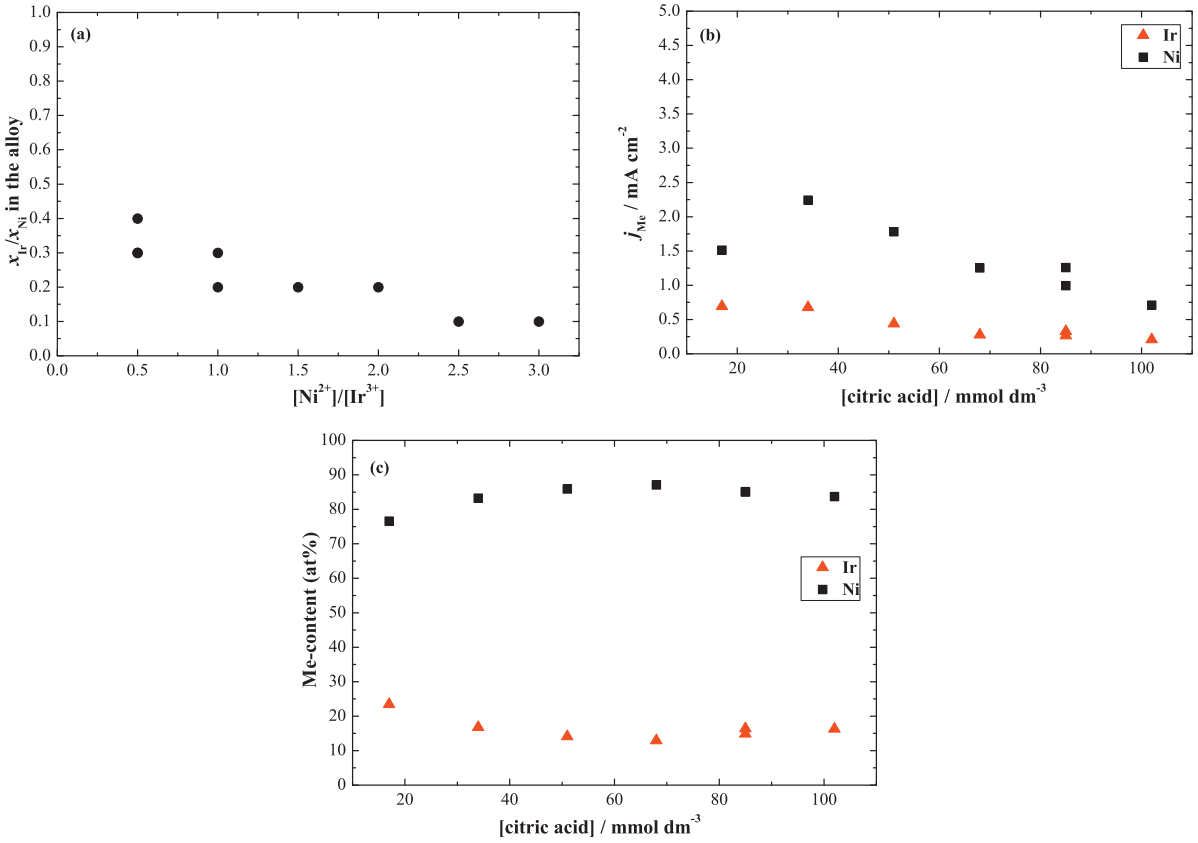

Fig. 4. (a) The Ir-to-Ni ratio in the alloy as a function of the Ni-to-Ir concentration ratio in the bath. (b) and (c) are the same as in Fig. 1, but in the absence of ReO_4^- ions in the bath.

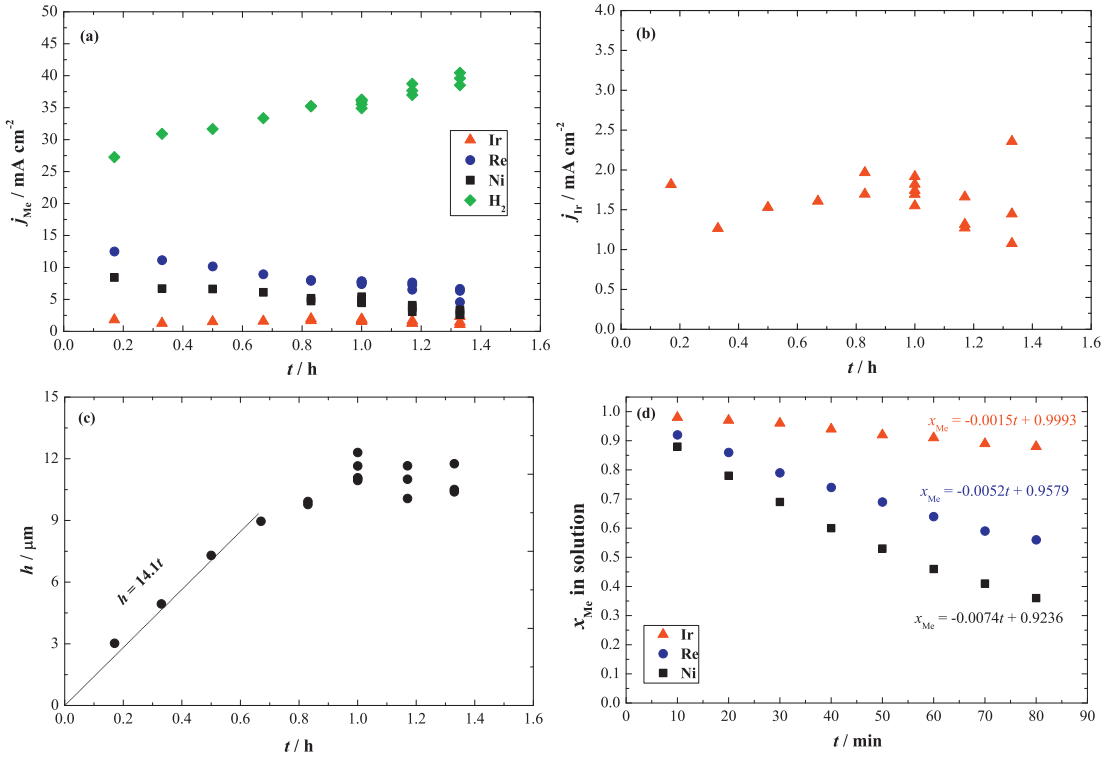

Fig. 5. The dependence of partial current densities of Me (a), partial current density of Ir in higher magnification (b), calculated thickness (c), and fraction of the metal ions in solution (d) on deposition time. Other variables, including the Ir^{3+} (34 mM), ReO_4^- (23 mM), Ni^{2+} (34 mM), and citric acid (34 mM) concentrations in the bath were kept constant.

Table 1
Bath compositions and operating conditions for selected samples.

Figure	t (min)	Bath composition (mM)				Sample number
		H_3Cit	$Ni(NH_2SO_3)_2$	$IrCl_3$	NH_4ReO_4	
6a	60	34	34	34	23	228
6b	60	17	34	34	23	116
6c	60	136	34	34	23	235
6d	60	34	136	34	23	205
6e	60	34	34	34	45	132
7a	60	34	51	17	23	154
7b	50	34	34	34	23	167

$T = 70 \pm 0.05$ °C, pH = 5.0 ± 0.05, and $j = 50$ mA cm^{-2}.

that the mechanism for the deposition of Re–Ni is also valid here. The conclusion that the deposition of Ir and Ni are two competing reactions taking place in parallel, combined with the finding that the rate of deposition of Ir is independent of the concentration of perrhenate, suggest a mechanism in which the reduction of Ni^{2+} and ReO_4^- occur in series, while the reduction of Ir as well as the reaction of hydrogen evolution occur in parallel. The reduction of the ReO_4^- ion is probably a multi-step complex process, taking the Re atom from a +7 valence state to the neutral atom. Moreover, this sequence must also include several proton-transfer steps, as shown by the overall reaction

$$ReO_4^- + 8H^+ + 7e^- \rightarrow Re^0 + 4H_2O \quad (6)$$

3.4. Coating characterization

3.4.1. Characterization of surface morphology, chemistry and coating thickness

The effect of bath chemistry and operating conditions on the chemical composition and surface morphology of the as-deposited Re–Ir–Ni coatings was evaluated by EDS and ESEM, respectively. Typical ESEM images of selected samples are shown in Fig. 6. The bath composition and operating conditions of representative samples for discussion are listed in Table 1. Characteristics of selected samples are presented in Table 2.

Fig. 6a shows the surface morphology of sample #228 that contains 27 at.% Re, 16 at.% Ir and 57 at.% Ni. A rather dense coating containing a net of micro-cracks is evident on the surface. These cracks may result either from hydrogen embrittlement or from residual stresses (associated, for example, with post-electrolysis decomposition of a hydride phase). Ohsaka et al. [20] attributed the crack formation to the absorption of hydrogen in the deposited coating. The formation of atomic hydrogen on the surface as an intermediate during plating is considered the worst aspect of hydrogen evolution and might lead to catastrophic failure of the coating [21]. In addition, Wu et al. [22] noted that the generation of hydrogen bubbles might impair the adhesion of the coatings. Eliaz [23] summarized several theories explaining the cracking in hard chromium deposits. The residual stresses were related to the way in which chromium grains crystallize, to the defects incorporated in the coating, or to volumetric contraction. Close examination of the surface in Fig. 6a reveals that it consists of globular regions with gaps in between. A surface morphology similar to that shown in Fig. 6a was found to be typical of most of the as-deposited coatings.

The surface morphology of sample #116 in Fig. 6b demonstrates the effect of decreasing the analytical concentration of citric acid in solution, while maintaining other conditions as in Fig. 6a. The composition of the deposited layer is essentially the same as in Fig. 6a. The FE is reduced by about 20%, and so is the thickness. Globular and cauliflower-like structures can be seen. A fine net of micro-cracks is also seen.

The effect of using an excess of citric acid on the surface morphology is shown, for sample #235, in Fig. 6c. The largest effect is on FE, which is lowered from 28% to 23% in Fig. 6a and b, respectively, to just 8% here. This can be attributed to the formation of a $[Ni(HCit)_2]^{2-}$ complex, which is known to sequester the Ni^{2+} ion, thus reducing the rate of its deposition. The surface of this sample appears to be smoother than the surfaces shown in Fig. 6a and b, but this may well be an artifact, resulting from the lower thickness of the deposit. One can note the larger micro-cracks and lower crack density as compared to those observed for lower concentrations of citric acid in Fig. 6a and b.

Fig. 6d shows the surface morphology of sample #205, for which the concentration of $Ni(NH_2SO_3)_2$ was increased to 136 mM. This leads to a large increase in the concentration of Re in the alloy, up to 73 at.%, showing the strong catalytic effect of the Ni^{2+} ion on the rate of deposition of Re. On the other hand, the Ir-content was decreased to only 1 at.%. This is consistent with the observation above (cf. Fig. 2b), indicating that deposition of Ni^{2+} and Ir^{3+} are competing reactions proceeding in parallel. This composition, having an excess of nickel ions, is interesting, because it yielded the highest Re concentration in the alloy, and one of the highest FE (42%) in the present study. Unfortunately, the concentration of Ir in the alloy formed is very low in this case. The surface morphology is significantly different from that in Fig. 6a. A continuous coating with smooth globules and relatively low density of cracks can be seen.

Fig. 6e demonstrates the structure of sample #132. The composition of the bath is the same as in Fig. 6a, except that the concentration of ReO_4^- is doubled. In general, the composition of the alloy and the FE are quite similar, but the surface morphology is different. The coating tends to peel-off and exhibits a lower crack density.

Backscattered electron (BSE) images of the metallographic cross-section of samples #154 and #167 are presented in Fig. 7a and b, respectively (note the different scale bars). The thickness of each coating was measured 5 times in 3 different fields of view. The thickness of sample #154 with a composition 35Re–5Ir–60Ni (at.%) was 16.1 ± 0.6 μm, while that of sample #167 with a composition 27Re–16Ir–57Ni was 9.5 ± 0.3 μm. The measured values of the thickness of the coatings are consistent with the calculated ones (obtained by weighing the sample before and after plating). Fig. 7a and b shows uniform, dense coatings with good adhesion to the substrate. The width of the cracks seems to be in the range of 0.1–1.0 μm, and some of them have propagated right across the coating to the substrate. They are a part of the network of cracks that were seen in all samples in the SEM.

The chemical composition of selected coatings was analyzed by XPS. The atomic concentrations of the elements at the surface before and after 10 min sputtering are listed in Table 3 for sample #228 (cf. Fig. 6a). On the surface, the elements O, C, N, Re, Ir and Ni were identified. After sputter cleaning, C and N disappeared, as expected. The concentration of oxygen at the surface of the coating decreased remarkably after short (1 min) sputtering, as shown in Fig. 8. Beyond 1 min of sputtering, only Ni, Re and Ir could be detected, and the concentration of these elements was essentially constant at longer sputtering. Hence, a thin layer of rhenium oxide had probably formed at the surface.

Table 2
Characteristics of selected samples. h is the coating thickness and w is the mass gain during deposition.

Sample number	ww (mg)	Ni (at.%)	Ir (at.%)	Re (at.%)	FE (%)	hh (μm)
228	26.4	57	16	27	28	11
116	22.4	54	18	28	23	9
235	7.2	37	16	48	8	3
205	33.1	26	1	73	42	11
130	25	56	14	30	27	10

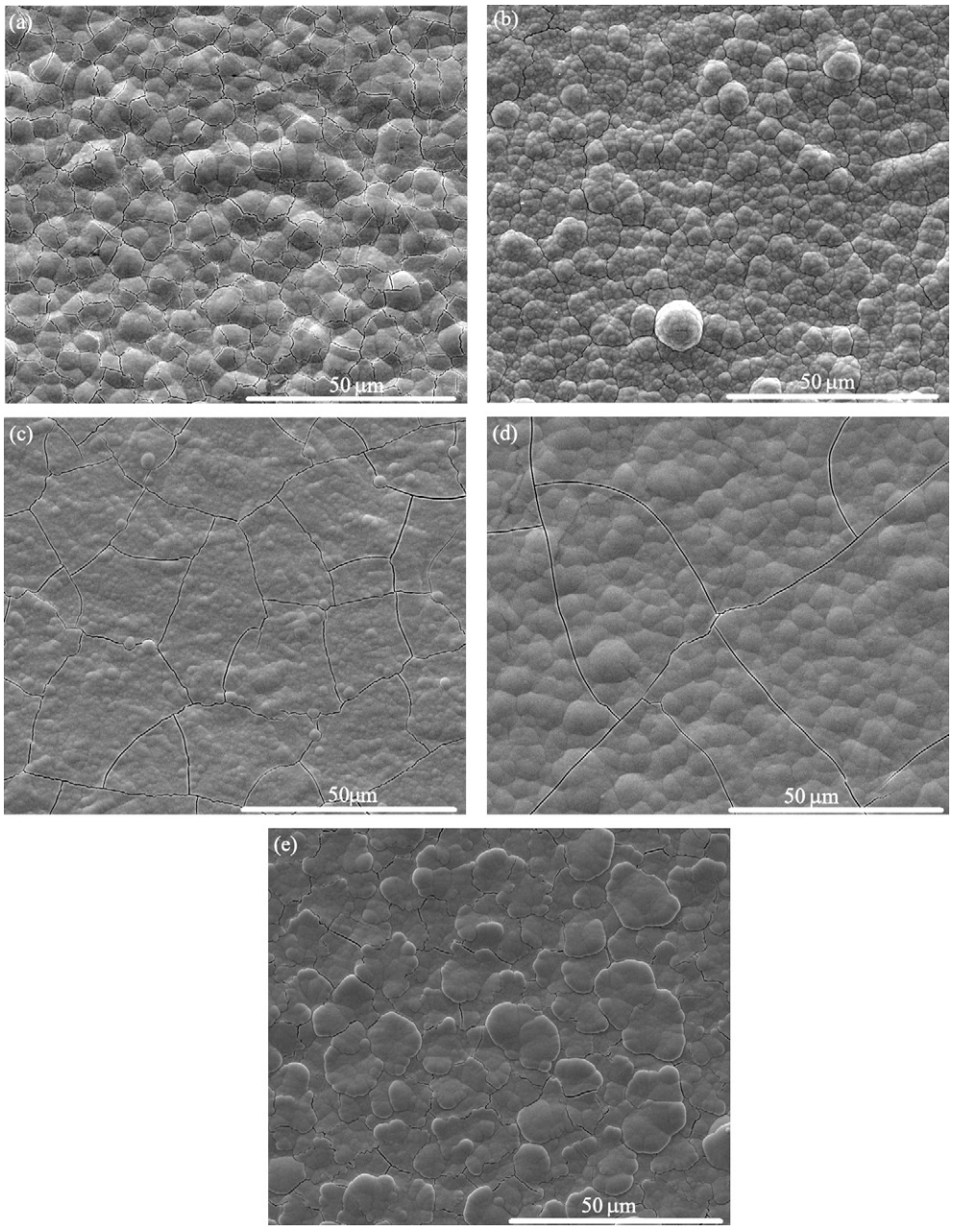

Fig. 6. ESEM secondary electron (SE) images of Re–Ir–Ni on copper substrate. Each image represents different process parameters (see Table 1 and text for more details).

Curve fitting was conducted to quantify and to deconvolve the contribution of each of the elements that comprise the alloy. Fig. 9 shows high-resolution XPS measurements of sample #228. The Re spectra before and after sputtering are shown in Fig. 9a and b, respectively, whereas those of Ir before and after sputtering are presented in Fig. 9c and d, respectively. Fitting of the Ir spectra was done with the aid of a reference foil made of pure Ir (20 min sputtered, O 1s = 1.28 at.%). The different states of Re, their quantities, and their peak positions, before and after sputtering, are summarized in Tables 4 and 5, respectively. The corresponding data for Ir is summarized in Tables 6 and 7.

Table 3
Atomic composition of sample #228 before and after sputtering, as determined by XPS.

Element	*c* (at.%)	
	After sputtering	Before sputtering
C	0	35.6
O	6.8	41.9
N	0	2.4
Re	38.6	8.3
Ir	22.2	2.5
Ni	32.4	9.3

Table 4
Peak positions and relative abundance (% out of at.% Re presented in Table 3) of oxidation states of Re at the surface of the coatings before sputtering.

Component	Peak positions ($4f_{7/2}$, eV)	FWHM (eV)	*c* (at.%)
Re	40.5	0.55	13.5
Re-alloy + O	41.01	1.5	19.5
ReO_2	42	1.3	5.3
Re_2O_5	43.5	1.3	7.1
ReO_3	44.77	1.3	7.6
ReO_4^-	46.28	1.28	47

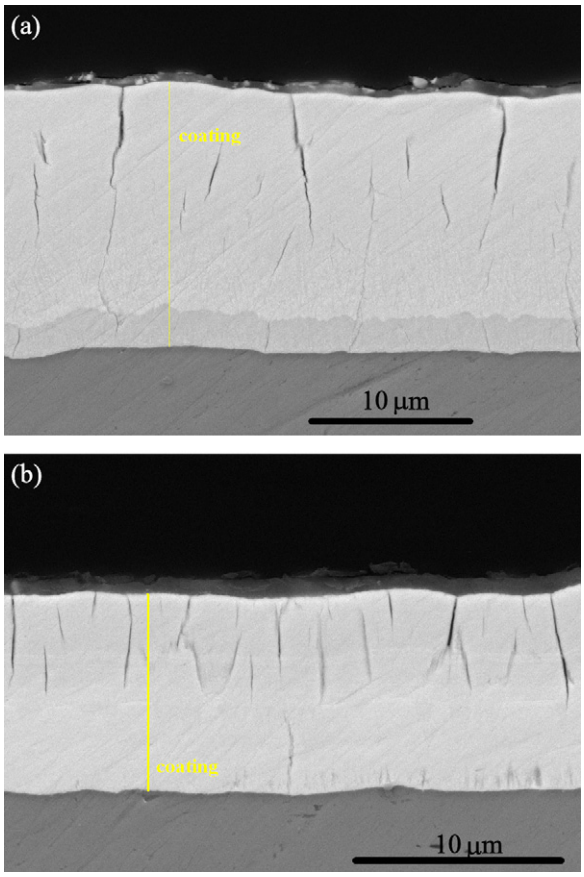

Fig. 7. ESEM backscattered electron (BSE) images acquired from metallographic cross-sections of two Re–Ir–Ni coatings on copper substrates. The samples are: (a) #154 and (b) #167 (see Table 1 and text for further details).

Table 5
Peak positions and relative abundance (% out of at.% Re presented in Table 3) of oxidation states of Re at the surface of the coatings after 10 min of sputtering.

Component	Peak positions ($4f_{7/2}$, eV)	FWHM (eV)	Chemical bond content (%)
Re	40.44	0.52	67.6
Re-alloy	40.77	0.66	17.1
Re-alloy + O	41.48	1.36	15.3

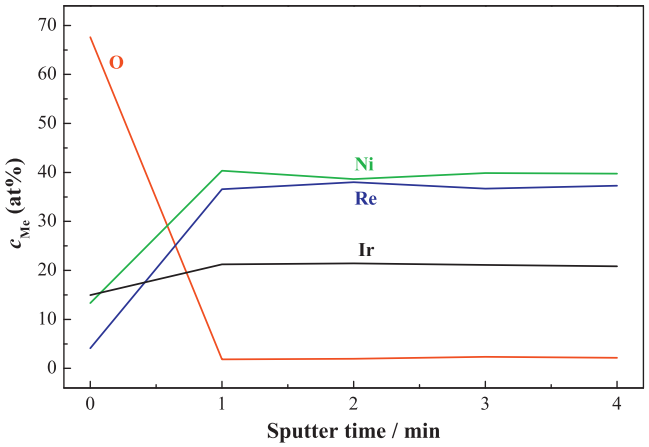

Fig. 8. XPS depth profiles for Re–Ir–Ni coating on Cu substrate (sample #228, see text for more details).

Table 6
Peak positions and relative abundance (% out of at.% Ir presented in Table 3) of oxidation states of Ir at the surface of the coatings before sputtering.

Component	Peak positions ($4f_{7/2}$, eV)	FWHM (eV)	Chemical bond content (%)
Ir-alloy	60.48	0.68	34.8
Ir	60.77	0.68	14.4
Ir-energy loss peak	60.97	1.53	37.1
IrO_2	62.52	1.23	13.7

Rhenium 4f and Ir 4f spectra are composed of doublet structures (2 peaks) due to multiplet splitting (i.e. $4f_{5/2}$ and $4f_{7/2}$). The peak positions of Re oxides are in good agreement with those detected in previous work [24]. The binding energy of Ir $4f_{7/2}$ was reported in other publications to be 60.8 eV and 60.7 eV [25,26]. Our results are in line with these reported values.

The change in chemical composition of Re after sputtering might be the result of a preferential sputtering effect. This effect, which is typical of heavy metal oxides, leads to oxygen depletion and appearance of lower oxidation states.

A doublet with Re $4f_{7/2}$ peak at 41.01 eV was detected before sputtering. Its binding energy is higher than that of Re, but lower than that of ReO_2. Therefore, it was concluded that this doublet corresponds to an oxidized state of Re-alloy + O. However, in the

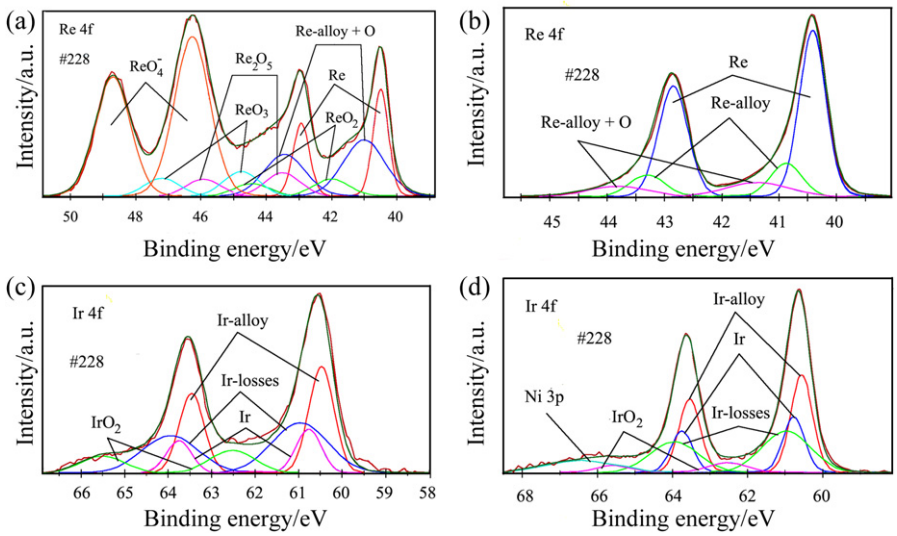

Fig. 9. High-resolution XPS measurements of sample #228 before (a and c) and after (b and d) sputtering. The peaks refer to Re 4f and Ir 4f.

Table 7
Peak positions and relative abundance (% out of at.% Ir presented in Table 3) of oxidation states of Ir at the surface of the coatings after 10 min of sputtering.

Component	Peak positions ($4f_{7/2}$, eV)	FWHM (eV)	Chemical bond content (%)
Ir-alloy	60.56	0.68	37.3
Ir	60.77	0.68	21.1
Ir-losses	60.97	1.53	34.8
IrO_2	62.52	1.23	6.8

absence of Re-foil reference it cannot be excluded that this peak could be related to loss of Re. There was no significant change in the peak position of Ni (0.05 eV) in the Ni 2p spectra before and after sputtering. This result indicates that there is no component of Ni-alloy in our system (see also Section 3.4.2).

The atomic concentrations of the elements after sputtering were somewhat different than those obtained by EDS. This discrepancy may be related to inhomogeneity of the as-deposited coatings or to preferential sputtering. It should be noted that a peak of Ni was also detected in the spectrum of Ir 4f due to overlapping of Ir 4f with a subsidiary peak of Ni 3p.

As evident in Fig. 9 b and d, XPS analysis revealed the presence of both Re and Ir alloys. A further investigation of this observation is presented in Section 3.4.2.

3.4.2. Crystallographic structure of the coatings

Fig. 10 shows the XRD patterns for selected samples of Re–Ir–Ni coatings on Cu substrates. The chemical composition and thickness of samples #228, #130 and #235 are given in Table 2. Indexing was made with reference to the JCPDS files for Cu (#00-004-0836), HCP $Ir_{0.4}Re_{0.6}$ (#97-010-4549 or #01-071-9295), HCP Ni (#01-089-7129), and hexagonal N_2H (#01-083-2378). FCC Ni, $Ir_{0.73}Re_{0.27}$ and other nickel hydrides were examined too, but it was concluded that neither of them was present in the coatings (unless their content was smaller than the sensitivity of the technique). Rhenium hydride, iridium hydride and Re–Ir–Ni phases were not included in the database, and therefore could not be taken into account in the analysis. The shift of some of the measured reflections relative to the JCPDS files may be associated with the non-powder character of the electrodeposited samples, different processing techniques, or distortions in the unit cell dimensions.

In Fig. 10, strong (2 0 0), (2 2 0) and (3 1 1) reflections from the Cu substrate are evident in the case of sample #235. This indicates that the coating is thin, which is consistent with the calculated thickness of 3 μm in Table 2. The black (bottom) indexing, which was made by standard comparison to the JCPDS files, shows that all other reflections may be attributed to the hexagonal nickel hydride,

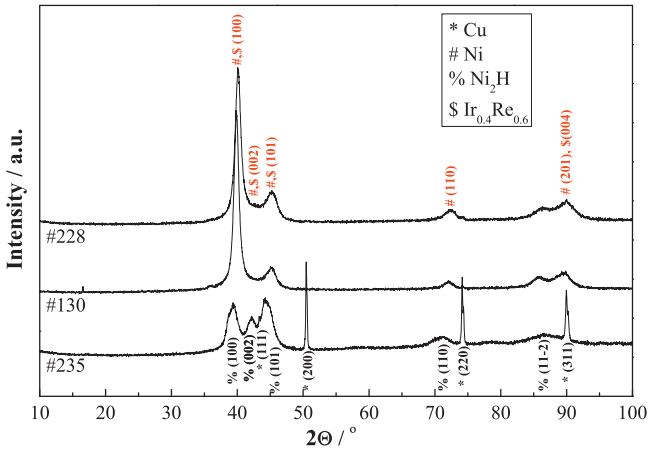

Fig. 10. XRD patterns of Re–Ir–Ni coating on Cu substrate.

Ni_2H. Post-electrolysis decomposition of this hydride to pure Ni would introduce residual stresses, which may be the cause of the cracking observed in Fig. 6.

However, a more sophisticated analysis, utilizing the WPF and Rietveld refinement techniques, resulted in the red (top) indexing. According to this analysis, all reflections from the coating may be attributed to HCP $Ir_{0.4}Re_{0.6}$ (space group $P6_3/mmc$) and HCP Ni (space group $P6_3/mmc$). These results are consistent with the XPS analysis.

The atomic radii of Re and Ir are 1.37 Å and 1.36 Å, respectively. Thus, Ir atoms can occupy substitutional sites of the HCP Re host lattice, thus forming a solid solution of Re–Ir-based alloy. The broad peaks indicate that very fine crystallites were formed, although peak broadening may be associated also with inhomogeneities in the composition of the alloy or with micro-strains. The size of the crystallites of the Re–Ir-based phase was in the range of 5–10 nm. For comparison, Karan et al. [27] reported Re–Ir nanoparticles with an average size of 3.3 nm. To the best of our knowledge, this is the first systematic observation of the formation of a Re–Ir-based phase electrochemically.

The HCP Ni nanoparticles showed a narrow size distribution around 5 nm. For comparison, Tzitzios et al. [28] have obtained HCP Ni particles in the range of 13–25 nm, while Gong et al. [29] synthesized HCP Ni with an average size of 12 nm. As the Ni-content in the alloy is increased from 37 at.% (sample #235) to 57 at.% (sample #228), a (1 0 0) preferred orientation, perpendicular to the substrate surface, is apparent.

Nickel is known to exist in two crystalline structures: FCC and HCP. However, in contrast to stable FCC Ni, the HCP Ni is a metastable phase [30]. Many studies have been focused on the synthesis of metastable HCP Ni by different methods and the characterization of its magnetic properties, compared to its equilibrium, ferromagnetic, FCC phase [28,30–32]. The HCP Ni was reported to be formed below a 4 nm critical crystalline size, or in thin films. In addition, it was found that the formation of metastable Ni structure depends on the substrate upon which it has been grown [33]. The formation of HCP Ni has been attributed to the incorporation of impurities such as C, N and H [34]. It was found that the HCP-to-FCC phase transformation occurs around 422 °C [30].

4. Conclusions

Electrodeposited Re–Ir–Ni coatings as thick as 18 μm, with Re-content as high as 73 at.% or Ir-content as high as 29 at.%, were obtained in different plating baths and under different operating conditions. The factors affecting the FE, the chemical composition of the alloy and the partial deposition current densities of each metal were studied. The following relations were identified:

1. The presence of citric acid in the bath exerts a considerable influence on the deposition process via the formation of various complexes with the metals. The FE and the partial current densities for Re, Ir and Ni deposition decrease as the concentration of citric acid is increased, except at low concentration of citric acid. By increasing the concentration of H_3Cit up to 136 mM, coatings with Re-content as high as 48 at.% were deposited, although at very low FE (8%).
2. The ReO_4^- concentration seems to have no significant effect on the partial current densities of Ir or Ni. This implies that the perrhenate anion does not take part in the rate-determining step for deposition of the alloy. It should be noted that this conclusion is far from being intuitively expected. Thus, while the reduction of Ni^{2+} or Ir^{3+} is a relatively simple process, complicated somewhat only by the possible formation of complexes with citrate, the reduction of the ReO_4^- ion must be a multi-step complex

process, taking the Re atom from a +7 valence state to the neutral atom.

3. As the concentration of Ni^{2+} in the solution was increased, coatings of high Re-content of 73 at.%, combined with a fairly high FE of 48%, were obtained. The Ni^{2+} ions in the plating bath exhibit a distinct catalytic effect on the rate of Re deposition, but not vice versa.
4. In contrast, increasing the Ni concentration in solution led to a significant decrease in the partial current density for deposition of Ir. We conclude that the deposition of Ni^{2+} and Ir^{3+} are competing reactions occurring in parallel. The presence of the ReO_4^- ion does not seem to influence the relationship between the Ni and Ir content in the alloy. On the other hand, the concentration of Ir^{3+} in the bath does not seem to have a catalytic effect on the rate of deposition of Re.
5. The effect of deposition time was studied. The mass gain showed a linear dependence on time up to 40 min, indicating a uniform deposition rate corresponding to 14.1 $\mu m\,h^{-1}$. At longer times the rate of deposition declines as a result of the low volume-to-surface ratio of the bath employed here, and is not inherent to the system.
6. The surface morphology was found to depend on the bath composition and operating conditions. Yet, a network of cracks was observed in all cases. Procedures for avoiding crack formation are a subject of further study in our laboratory.
7. The ternary Re–Ir–Ni coatings consisted of two phases with nanometric crystallites: an HCP $Ir_{0.4}Re_{0.6}$ phase and an HCP Ni phase. The formation of a hexagonal nickel hydride phase is also possible. To the best of our knowledge, this is the first observation of the electrochemical formation of a Re–Ir-based phase.

Acknowledgements

This research was conducted with financial support from the US Air Force Office of Scientific Research (AFOSR, grant number FA9550-10-1-0520) as well as from the Israel Department of Defense (grant number 4440258441). The authors thank Dr. L. Burstein, Dr. Yu. Rosenberg and Dr. Z. Barkay from the Wolfson Applied Materials Research Center at Tel-Aviv University for their help in XPS, XRD and ESEM work, respectively. We also thank M. Levenshtein for his help in preparation of metallurgical cross-sections.

References

[1] N. Eliaz, E. Gileadi, Induced codeposition of alloys of tungsten, molybdenum and rhenium with transition metals, in: C.G. Vayenas, R.E. White, M.E. Gamboa Aldeco (Eds.), Modern Aspects of Electrochemistry, vol. 42, Springer, New York, 2008, p. 191 (Chapter 4).
[2] A. Naor, N. Eliaz, E. Gileadi, S.R. Taylor, Properties and applications of rhenium and its alloys, AMMTIAC Quarterly 5 (2010) 11.
[3] J.R. Davis (Ed.), ASM Specialty Handbook: Heat-Resistant Materials, ASM International, Materials Park, 1997.
[4] B.D. Reed, J.A. Bigalow, S.J. Schneider, Engineering issues of iridium coated rhenium rockets, Materials and Manufacturing Processes 13 (1998) 757.
[5] R.H. Tuffias, Fabrication processes for iridium/rhenium combustion chambers, Materials and Manufacturing Processes 13 (1998) 773.
[6] http://www.nasa.gov/centers/glenn/pdf/168206main_CenterResume.pdf (accessed 14.10.12).
[7] J.R. Vargas Garcia, T. Goto, Chemical vapor deposition of iridium, platinum, rhodium and palladium, Materials Transactions 44 (2003) 1717.
[8] N. Eliaz, T.M. Sridhar, E. Gileadi, Synthesis and characterization of nickel tungsten alloys by electrodeposition, Electrochimica Acta 50 (2005) 2893.
[9] A. Naor, N. Eliaz, E. Gileadi, Electrodeposition of alloys of rhenium with iron-group metals from aqueous solutions, Journal of the Electrochemical Society 157 (2010) D422.
[10] A. Naor, N. Eliaz, E. Gileadi, Electrodeposition of alloys of rhenium with iron-group metals from aqueous solutions, Electrochemical Society Transactions 25 (2010) 137.
[11] A. Naor, N. Eliaz, E. Gileadi, Electrodeposition of rhenium-nickel alloys from aqueous solutions, Electrochimica Acta 54 (2009) 6028.
[12] G.A. Conn, Iridium plating, Plating and Surface Finishing 52 (1965) 1258.
[13] D.A. Fine, On the spontaneous reduction of hexachloroiridate(IV) in aqueous solution, Inorganic Chemistry 8 (1969) 1014.
[14] D.A. Fine, Studies of the iridium(III) and (IV)—chloride system in acid solution, Journal of Inorganic and Nuclear Chemistry 32 (1970) 2731.
[15] T. Jones, Iridium plating, Met. Finish 102 (6) (2004) 87;
T. Jones, Electrodeposition of the Lesser-Known Precious Metals: Osmium, Iridium, Rhodium, Rhenium, Ruthenium, rev. ed., Finishing Publications Ltd., Stevenage, 2005.
[16] R.B. King, Encyclopedia of Inorganic Chemistry, vol. 3, Wiley, Chichester, 1994, p. 1606.
[17] J.J. Vajo, D.A. Aikens, L. Ashley, D.E. Poeltl, R.A. Bailey, H.M. Clark, S.C. Bunce, Facile electroreduction of perrhenate in weakly acidic citrate and oxalate media, Inorganic Chemistry 20 (1981) 3328.
[18] A. Duhin, A. Inberg, N. Eliaz, E. Gileadi, Electroless plating of rhenium–nickel alloys, Electrochimica Acta 56 (2011) 9637.
[19] A. Naor-Pomerantz, N. Eliaz, E. Gileadi, Electrodeposition of rhenium-tin nanowires, Electrochimica Acta 56 (2011) 6361.
[20] T. Ohsaka, M. Isaka, K. Hirano, T. Ohishi, Effect of ultrasound sonication on electroplating of iridium, Ultrasonics Sonochemistry 15 (2008) 283.
[21] E. Gileadi, Physical Electrochemistry, Fundamentals, Techniques and Applications, Wiley-VCH, Weinheim, 2011.
[22] F. Wu, H. Murakami, Y. Yamabe-Mitarai, H. Harada, H. Katayama, Y. Yamampto, Electrodeposition of Pt–Ir alloys on nickel-base single crystal superalloy TMS-75, Surface and Coatings Technology 184 (2004) 24.
[23] N. Eliaz, Comparison between the conventional and high-efficiency hard chromium platings in regard to aeronautical demands, Journal of Advanced Materials 33 (2001) 27.
[24] A. Naor, N. Eliaz, L. Burstein, E. Gileadi, Direct experimental support for the catalytic effect of iron-group metals on electrodeposition of rhenium, Electrochemical and Solid-State Letters 13 (2010) D91.
[25] J.C. Fuggle, N. Mhrtensson, Core level binding energies in metals, Journal of Electron Spectroscopy 21 (1980) 275.
[26] S. Hufner, G.K. Wertheim, Core-line asymmetries in the x-ray-photoemission spectra of metals, Physical Review B 11 (1975) 678.
[27] H. Karan, K. Sasaki, K. Kuttiyiel, C.A. Farberow, M. Mavrikakis, R.R. Adzic, Catalytic activity of platinum monolayer on iridium and rhenium alloy nanoparticles for the oxygen reduction reaction, ACS Catalysis 2 (2012) 817.
[28] V. Tzitzios, G. Basina, M. Gjoka, Chemical synthesis and characterization of hcp Ni nanoparticles, Nanotechnology 17 (2006) 3750.
[29] J. Gong, L.L. Wang, Y. Liu, J.H. Yang, Z.G. Zong, Structural and magnetic properties of hcp and fcc Ni nanoparticles, Journal of Alloys and Compounds 457 (2008) 6.
[30] A. Lahiri, Z. Tadisina, Synthesis, thermodynamic and magnetic properties of pure hexagonal close packed nickel, Materials Chemistry and Physics 124 (2010) 41.
[31] A. Lahiri, R. Das, R.G. Reddy, Electrochemical synthesis of hexagonal closed pack nickel: A hydrogen storage material, Journal of Power Sources 195 (2010) 1688.
[32] J.G. Wright, J. Goddard, The lattice constants and magnetic anisotropy constants of electrodeposited single crystal films of hexagonal close-packed nickel, Philosophical Magazine 11 (1965) 485.
[33] A.S. Bolokang, M.J. Phasha, Novel synthesis of metastable HCP nickel by water quenching, Materials Letters 65 (2011) 59.
[34] Y. Mi, D. Yuan, Y. Liu, J. Zhang, Y. Xiao, Synthesis of hexagonal close-packed nanocrystalline nickel by a thermal reduction process, Materials Chemistry and Physics 89 (2005) 359.